Constraint Effect in Fracture: Investigation of Cruciform Specimens using the J-A_2 Method

Larry Sharpe[1], Yuh Chao[2,*]

[1] Department of Mechanical Engineering University of Tennessee, Knoxville, TN, USA
[2] College of Material Science and Engineering, Tianjin University, Tianjin, China
* Corresponding author: chao@sc.edu

Abstract
The structural integrity of cracked mechanical components can be assessed using the fracture toughness material property. The fracture toughness of a particular component is often dependent upon the component geometry as well as the nature of loading (e.g. uniaxial or biaxial loading). This dependence is interpreted as the constraint effect in fracture. Various methods have been developed to investigate the constraint effect, including the two parameter J-A_2 method. The J-A_2 method is a more accurate representation of the stress fields near the crack tip, as additional terms from the well-known HRR series solution are included. The current study applies the J-A_2 method to fracture toughness data of cracked cruciform specimens subjected to uniaxial and biaxial stresses. The J-A_2 results of the cruciform specimens are compared to those of other plane strain specimens described by ASTM standards, including three point bend and compact tension, to determine if loss of constraint exists. Finite element models of each specimen were analyzed to determine the A_2 parameter used to quantify the level of constraint based on geometry and loading. The results reveal loss of constraint for shallow cracked specimens when compared to deep cracked specimens, and also that uniaxial loading results in loss of constraint when compared to biaxial loaded specimens. In summary, the J-A_2 method appears to be a viable tool to predict failure including the consideration of the constraint effect.

Keywords fracture, constraint, biaxial, cruciform

1. Introduction

A material's fracture toughness is used to determine the structural integrity of mechanical components containing cracks. Materials used in nuclear reactor pressure vessels (RPV), including A533B and A508, are of particular interest. RPVs can be subjected to conditions close to equibiaxial loading during extreme temperature gradients experienced during pressurized thermal shock (PTS).

Based on such biaxial loading, it is possible that traditional methods used to determine material properties may not provide accurate results. Widely used industry standards [1, 2] used to calculate material properties related to fracture toughness utilize specimens subjected to uniaxial loading, e.g., three point bend (3PB) and compact tension (CT) specimens. Therefore, the question arises regarding whether or not a "biaxial effect" exists for loading conditions similar to that of RPVs.

Much research has been conducted in recent years to determine how component geometry and applied loading affect fracture toughness. The industry standards mentioned previously typically use deep cracked (high constraint) specimens to determine the fracture toughness. But it is known that shallow cracked (low constraint) specimens exhibit higher fracture toughness, resulting in a "constraint effect" in fracture.

The current study uses a two-parameter method to quantify the constraint of a variety of specimens and also to predict failure of specimens of biaxial loads. The J-A_2 method has been applied to experimental data published by the Fraunhofer Institute for Mechanics. Fraunhofer conducted fracture toughness testing on 3PB and cruciform specimens, with the cruciform specimens subjected to biaxial loads. Such experimental data can be used to determine if the J-A_2 method can be used as a tool to i) predict failure of mechanical components of different constraints and ii) quantify the constraint due to loading and geometry.

2. J-A_2 Two Parameter Method

The stress distribution ahead of the crack tip described by the well-known HRR solution [3, 4] is

$$\sigma_{ij} = \sigma_0 \left(\frac{J}{\alpha \varepsilon_0 \sigma_0 I_n r} \right)^{1/n+1} \tilde{\sigma}_{ij}(\theta, n), \qquad (1)$$

where σ_0 is a reference (or yield) stress, $\varepsilon_0 = \sigma_0 / E$ is a reference (or yield) strain, E is Young's modulus, α is a material constant, and n is the strain-hardening exponent. The integration constant I_n and the dimensionless angular functions of stresses $\tilde{\sigma}_{ij}$ depend on the strain-hardening exponent. Equation 1 is the first term of a series solution. Further, the HRR solution described by Equation 1 is defined by only one parameter, the J-integral, which is related to the energy release rate around the crack tip during loading. As shown in Figure 1, the stress field as described by the HRR solution is valid as $r \to 0$. In theory, the stress approaching the crack tip increases asymptotically to infinity, meaning a component subjected to such stress would fail under very small loads.

In practice, this is typically not the case, especially with materials exhibiting elastic-plastic behavior. The HRR solution does not consider large deformations or blunting of the crack and is only valid for small strains as $r \to 0$. An example of the actual stress field near the crack tip is also shown in Figure 1. Ritchie, et al. [5] determined that cleavage fracture actually occurs at some critical distance (r_c) when the stress at that location exceeds the critical stress (σ_c) and this failure criterion is often referred to as the RKR model.

Clearly, the single term HRR solution can overestimate the actual stress ahead of the crack tip. As a result, various procedures have been developed to include additional terms from the series expansion. Yang et al. [6, 7] and Chao et al. [8] developed an asymptotic crack-tip solution using three terms of the series solution from which the HRR solution is derived. The *J-A_2* procedure uses two parameters to better define the stress ahead of the crack tip. The *J*-integral is representative of the magnitude of the applied loading, while the A_2 term is used to describe the constraint at the crack tip based on the loading and specimen geometry.

The procedure begins by using the Ramberg-Osgood power-law relationship for a strain-hardening material for a Mode I crack under plane strain conditions. The Ramberg-Osgood equation relating uniaxial strain ε to the uniaxial stress σ in tension is

$$\frac{\varepsilon}{\varepsilon_0} = \frac{\sigma}{\sigma_0} + \alpha \left(\frac{\sigma}{\sigma_0} \right)^n . \qquad (2)$$

Eq. 2 can be rewritten in general terms by applying the J_2 deformation theory of plasticity

$$\frac{\varepsilon_{ij}}{\varepsilon_0} = (1+\nu)\frac{\sigma_{ij}}{\sigma_0} - \nu\frac{\sigma_{kk}}{\sigma_0}\delta_{ij} + \frac{3}{2}\alpha\left(\frac{\sigma_e}{\sigma_0}\right)^{n-1}\frac{s_{ij}}{\sigma_0}, \qquad (3)$$

where ν is the Poisson's ratio, δ_{ij} is the Kronecker delta, s_{ij} is the deviatoric stress, and σ_e is the von Mises effective stress defined as $\sigma_e = \sqrt{3\,s_{ij}s_{ij}/2}$. The asymptotic stress field can then be expressed as

$$\frac{\sigma_{ij}}{\sigma_0} = A_1\left[\left(\frac{r}{L}\right)^{s_1}\tilde{\sigma}_{ij}^{(1)}(\theta,n) + A_2\left(\frac{r}{L}\right)^{s_2}\tilde{\sigma}_{ij}^{(2)}(\theta,n) + A_2^{\,2}\left(\frac{r}{L}\right)^{s_3}\tilde{\sigma}_{ij}^{(3)}(\theta,n)\right], \qquad (4)$$

The angular stress functions and the stress power exponents are functions solely of the hardening exponent and are independent of the applied load and any material properties. The characteristic length, L, in Equation 4 is typically assigned one of the primary dimensions of the specimen under investigation; possibilities include the crack length, the specimen width, the specimen thickness, or even unity. For the current study, L = 1 mm for all cases. The parameters A_1 and s_1 from Equation 4 are related to the HRR solution (Eq. 1) by

$$A_1 = \left(\frac{J}{\alpha\varepsilon_0\sigma_0 I_n L}\right)^{-s_1}, \quad s_1 = -\frac{1}{n+1}, \qquad (5)$$

Comparing Eq. 4 and 1, it can be seen that the first term of the two-parameter equation (Eq. 4) is the same as the HRR solution (Eq. 1). Further, the additional stress power exponents can be calculated using $s_3 = 2s_2 - s_1$ for $n \geq 3$. Thus, the final stress power exponent, s_2, can be calculated numerically.

An apparent application of the J-A_2 method is to use the two parameters to predict failure of flawed components. Chao et al. [9] described the development of Material Failure Curves by plotting J-integral values versus the absolute value of A_2 (J vs. $|A_2|$), as A_2 is always a negative value. Using a modified version of Equation 4,

$$\frac{\sigma_c}{\sigma_0} = A_1\left[\left(\frac{r_c}{L}\right)^{s_1}\tilde{\sigma}_{ij}^{(1)}(\theta,n) + A_2\left(\frac{r_c}{L}\right)^{s_2}\tilde{\sigma}_{ij}^{(2)}(\theta,n) + A_2^{\,2}\left(\frac{r_c}{L}\right)^{s_3}\tilde{\sigma}_{ij}^{(3)}(\theta,n)\right], \qquad (6)$$

the aforementioned critical stress (σ_c) and corresponding critical radial distance (r_c) from the RKR model are substituted and J and A_2 can be determined and plotted. According to the RKR model, the location where failure initiates, r_c, occurs in the range of 2-4 grain diameters ahead of the crack. This equates to 0.12mm to 0.24mm for A533B, or $1 < r/(J/\sigma_0) < 5$ where $r/(J/\sigma_0)$ is the normalized radial distance ahead of the crack. Once σ_c and r_c have been determined, the critical values can be used in Equation 6 to plot a Material Failure Curve as shown in the left portion of Fig. 1.

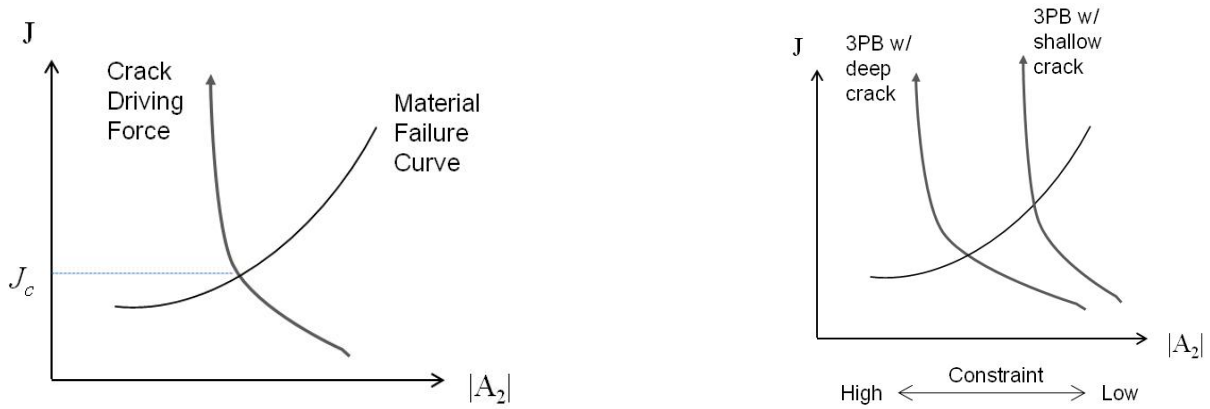

Figure 1. J vs. $|A_2|$ with Material Failure Curve and Crack Driving Force curve (left) and comparison of constraint levels (right)

The J vs. $|A_2|$ plot can be used to predict failure of components when the Crack Driving Force curve is added. The Crack Driving Force curve is a plot of multiple (J, $|A_2|$) pairs at any applied load, not just at the critical values. The intersection of the Material Failure Curve and the Crack Driving Force defines the critical J value (J_c) at which cleavage fracture will occur and can be used to predict the load at failure.

The J vs. $|A_2|$ plot can also be used to determine the constraint effect of specimens with different geometries and loading configurations. An example is shown in right diagram of Fig. 1. Crack Driving Force curves for 3PB specimens are shown on the J vs. $|A_2|$ plot. Specimens with deep cracks are high constraint specimens and typically exhibit lower fracture toughness than shallow cracked specimens. It should be noted that constraint is a relative term. A_2 provides a quantitative measure of constraint, although the magnitude of A_2 is of little value. The A_2 value of one specimen is simply compared to the A_2 value of other specimens to determine if there exists "loss of constraint" or, rather, an increase in fracture toughness.

3. Fraunhofer Experimental Data

3.1. Background

A set of published results to which the J-A_2 method could be applied were found in journal articles [10, 11] published by a team of researchers from the Fraunhofer Institute for Mechanics of Materials. These specimens and results presented in the article will be hereinafter referred to as the "Fraunhofer" specimens and results.

The goal of the Fraunhofer research was to determine the fracture toughness of a variety of cracked specimens. Specimens were tested over a wide range of lower shelf temperatures. Many trials with 3PB, C(T), and cruciform specimens were conducted at -85°C. The Fraunhofer cruciform specimen is shown below in Fig. 2. The cross sectional area of the small-scale cruciform arms

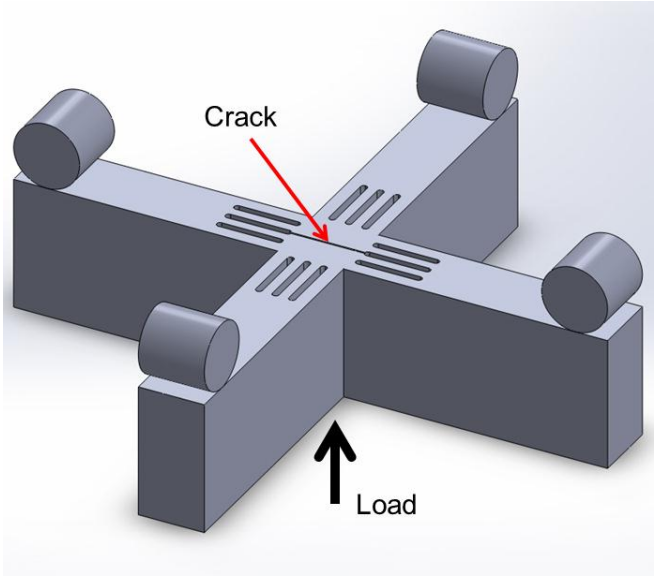

Figure 2. Fraunhofer cruciform specimen with five-point bending to simulate biaxial loading of crack

is only 10 mm x 20 mm (B = 10 mm and W = 20 mm). The distance between the roller supports in the five point bending test rig is 80 mm, while the overall dimensions of the specimen are 90 mm x 90 mm.

Also, smaller scale 3PB specimens are incorporated as well. The Fraunhofer study used pre-cracked Charpy test specimens rather than standard 3PB specimens specified in ASTM E1921 [2]. The 3PB specimens contained shallow cracks (a/W = 0.18). Standard 1T-C(T) specimens (a/W = 0.5) were also tested. Testing of such small specimens is completed in an effort to determine if the fracture toughness results are applicable to much larger scale components, including reactor pressure vessels.

3.2. Material Properties

The Fraunhofer specimens were machined from a section of A508 Class 2 steel, commonly used to fabricate reactor pressure vessels. Material properties for A508 were obtained from another recent study conducted by Scibetta et al. [12]. The researchers provided the following equation to correct the yield stress (in MPa) based on temperature (T, in degrees Celsius)

$$\sigma_{YS} = 398 + 45.2\exp(-0.01413\,T) \tag{7}$$

In addition, Scibetta et al. [12] also presented a temperature correction for E (in GPa) again where the temperature is in degrees Celsius,

$$E = 207 - 0.06\,T \tag{8}$$

Thus, at -85°C, the yield stress and Young's modulus were determined to be 550 MPa and 212.1 GPa, respectively. Poisson's ratio was assumed to be 0.3 as typical with many steels.

The Fraunhofer study [11] provided true stress vs. true strain curves for the material. A curve fitting procedure was used to determine the strain hardening exponent necessary for the elastic-plastic finite element analysis using the Ramberg-Osgood equation. The strain hardening exponent was determined to be n = 8. The angular stress functions and the stress power exponents

necessary to solve the two-parameter J-A_2 equation (Eq. 4) are provided in tables developed by Chao et al. [13].

3.3. Finite Element Analysis Models

The FEA models developed using Abaqus [14] for the 3PB and 1T C(T) specimens are shown below in Fig. 3.

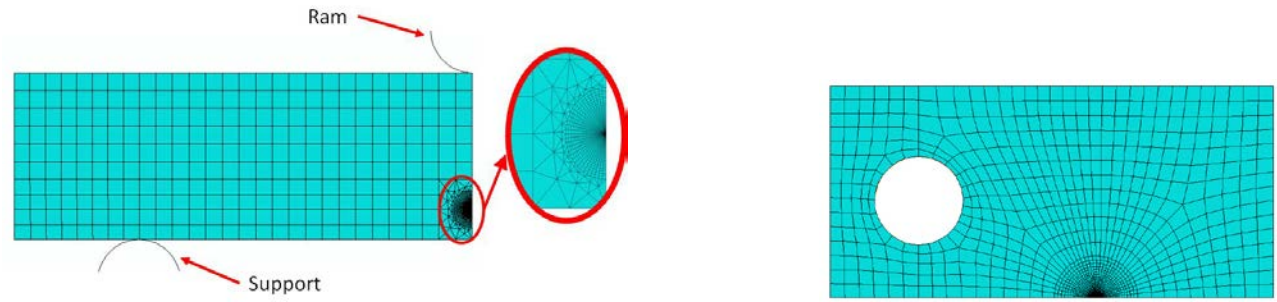

Figure 3. FEA mesh for Fraunhofer 3PB specimen (left) and 1T C(T) specimen (right).

Both meshes are composed mostly of eight node CPE8R quadratic plane strain elements, The extremely fine mesh around the crack tip includes elements with width of 0.001mm necessary to capture A_2 within the range of $1 < r/(J/\sigma_0) < 5$. The innermost ring of elements at the crack tip is comprised of eight node wedge elements with collapsed nodes at the tip to allow for blunting of the crack and large scale deformation.

The Fraunhofer cruciform is a small scale specimen. The overall dimensions are 90 mm x 90 mm. The specimen is machined with a shallow crack such that the crack depth ratio $a/W = 0.08$. The cruciform is tested in a five point bending configuration. In addition, two of the roller supports can be adjusted to allow for varying biaxiality ratios. However, only 1:1 biaxial loading was tested at the -85°C test temperature.

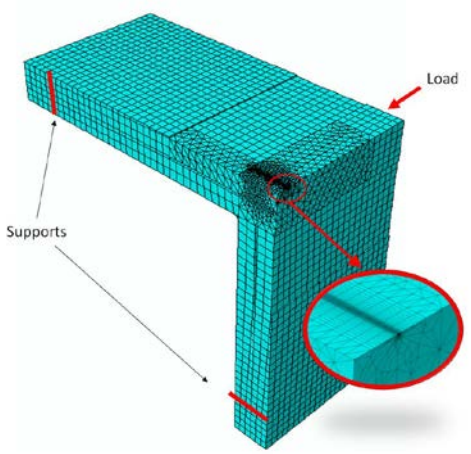

Figure 4. FEA mesh for Fraunhofer cruciform specimen

The cruciform specimen mesh shown in Fig. 4 contains 20,174 elements composed mostly of 20 node quadratic hexahedral C3D20R 3-D stress elements with a focused mesh around the crack tip. Elements in the focused mesh region are as small as 0.001 mm in order to capture the stress field in the region of cleavage fracture as defined by the RKR model. The average fracture toughness (J_c)

of the Fraunhofer biaxial cruciform specimens was determined to be 85.7 N/mm.

3.4. J-A_2 Method Applied to Fraunhofer Test Data

Loads were applied to the 3PB and C(T) FEA models until the J_c values presented in Table 1 were achieved. The stress (obtained from FEA output) perpendicular (i.e., $\theta = 0°$) to the crack front at a node ahead of the crack tip, along with radial position, r, of the node and J_c, can be substituted into Equation 4 to solve the quadratic equation for A_2 at each node. Again, according to the RKR model, fracture typically initiates within the range $1 < r/(J/\sigma_0) < 5$. Thus, A_2 was calculated at each node within this range and the average was tabulated. For this study, the average was actually taken approximately for the range $2 < r/(J/\sigma_0) < 5$ i.e., the first few nodes adjacent to the crack tip were neglected for the average A_2 calculation. The A_2 results are also summarized in Table 2 in the form of (J_c, A_2) pairs.

Table 1. (J_c, A_2) pairs for the 3PB and C(T) specimens

J_c is in N/mm, A_2 is unitless	
	-85°C
3PB shallow (a/W = 0.18)	(54.2, -0.392)
1T-C(T) (a/W = 0.5)	(13.1, -0.260)

Next, using the (J_c, A_2) pair for the 3PB specimen, and substituting the published value of σ_c = 1830 MPa [15, 16], Equation 6 can be used to solve for the fracture initiation location r_c, which is 0.104 mm for both specimens, a value which is in agreement with other published results. A study conducted by Wang et al. [17] focused on the determination of the fracture initiation location and they determined that, for temperatures in this range, r_c lies within the range of 0.1 mm to 0.25 mm. Additional evidence of an appropriate range of r_c values was found in [18], in which dozens of data points for the similar A508 material yielded 0.05 mm < r_c < 0.25 mm. Substituting r_c and σ_c into Equation 5, the Material Failure Curve can be plotted.

The FEA models are processed with incremental loads to determine a range of J values above and below J_c such that the Crack Driving Force curves for each specimen can be determined. The Material Failure Curve and Crack Driving Force curves are then plotted on the same J vs. $|A_2|$ plot. As the loading increases, the applied J increases from zero. And, therefore, referring to Figure 2, points on the plot above and left of the Material Failure Curve indicate fracture has occurred. Crack Driving Force curves, as shown in Figure 3, are indicative of each specimen's constraint and can be used to determine if the desirable "loss of constraint" occurs, i.e., fracture toughness increases due to geometry and/or loading conditions. The J vs. $|A_2|$ plot for the specimens is shown in Fig. 5. The triangles are actual data points obtained from the Fraunhofer study.

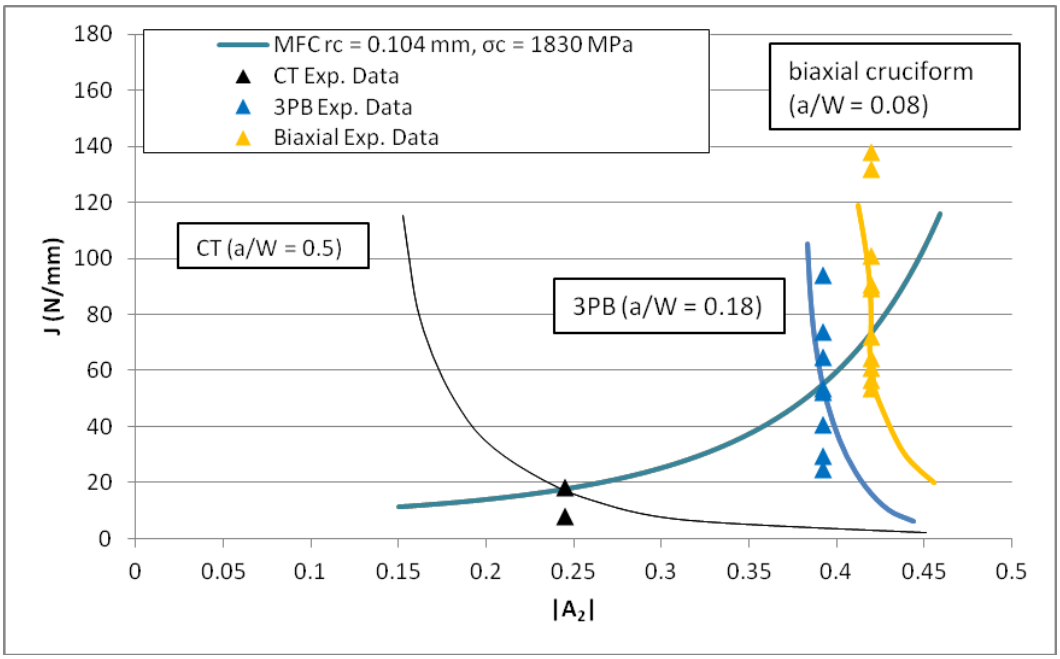

Figure 5. Material Failure Curve and Crack Driving Force curves for the Fraunhofer specimens (A508 material) at -85°C

4. Discussion of Results

The results presented in Fig. 5 reveal that the two parameter J-A_2 method does have the potential to i) predict failure, and ii) quantify constraint. The 3PB and biaxial cruciform specimens reveal significant loss of constraint when compared to the high constraint C(T) specimen. The biaxial cruciform exhibits higher fracture toughness (lower constraint) than the 3PB specimen. This may be attributed to the fact that the crack depth of the biaxial cruciform (a/W = 0.08) is more than twice as shallow as the 3PB specimen (a/W = 0.18), which may have overshadowed the biaxial effect. This supports the findings of Lidbury et al. [19] of a shallow crack effect.

Fig. 5 also shows the experimental fracture toughness data [10, 11] added to the Crack Driving Force curves in the form of the triangular symbols. The experimental fracture toughness data has been added at the $|A_2|$ values corresponding to the predicted critical $|A_2|$ to be compared with the Crack Driving Force curves. The average values of the experimental fracture toughness for all three specimens lies near the intersection of the MFC and the specimen CDFs. The constraint effect of each of the specimens can also be quantified and compared using the Crack Driving Force curves. The Crack Driving Force curves in Fig. 5 for the biaxial loading lies to the right of the 3PB specimen, meaning some loss of constraint and increased fracture toughness based on the loading and geometry.

For the purposes of comparing the fracture toughness values, a similar FEA and J-A_2 analysis of a uniaxial cruciform was conducted as part of the current investigation. The supports in the FEA model on the cruciform arms parallel to the crack, i.e., the horizontal arms shown in Fig. 2, were removed to simulate uniaxial loading. The same procedure was followed to develop the Crack Driving Force curve for the theoretical uniaxial cruciform specimen, which is shown as the red curve in Fig. 6. Clearly, the uniaxial cruciform specimen exhibits significant loss of constraint (increased fracture toughness) compared to the biaxial cruciform specimen.

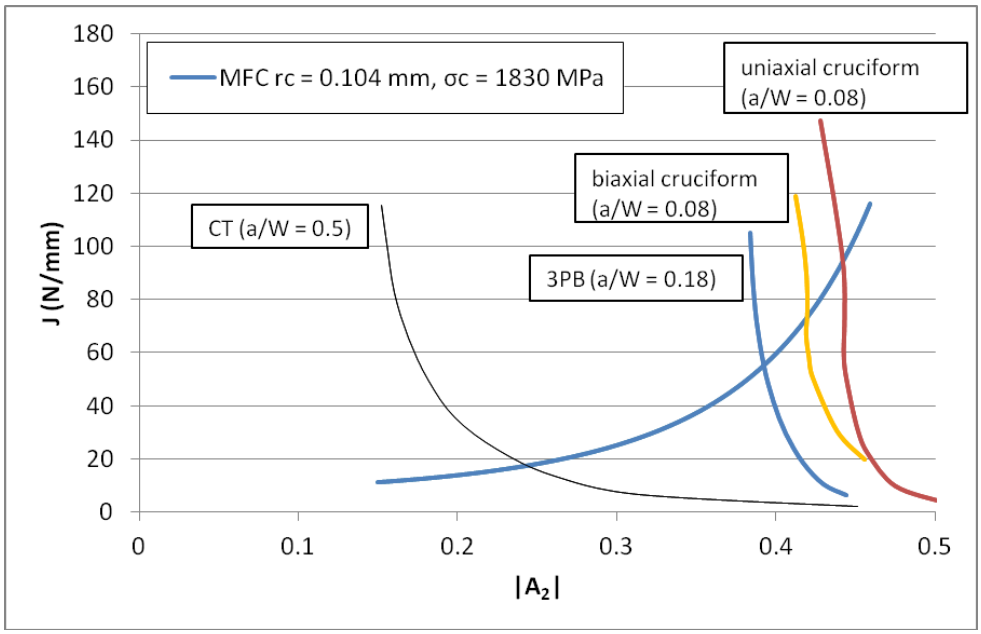

Figure 6. Crack Driving Force curve for theoretical uniaxial cruciform specimen indicated by the red curve (A508 material at -85°C)

The fracture toughness (J_c indicated by the intersection of the MFC and CDF) of the uniaxial cruciform specimen is estimated to be around 92 N/mm, while the fracture toughness of the biaxial cruciform is approximately 75 N/mm. In addition, the 3PB specimen has a slightly deeper crack than the cruciform specimens, therefore its fracture toughness is much less. The uniaxial specimen shows slightly greater loss of constraint (higher fracture toughness) when compared to biaxial specimens. This agrees with findings published by AREVA [20] related to RPV integrity assessment.

5. Conclusion

The two parameter J-A_2 method has been applied to experimental data obtained from testing A508B 3PB, C(T), and small scale cruciform specimens. The J-A_2 method shows great potential for use to predict failure in structural components and also to quantify the constraint effect due to varying loading and geometry. However, additional work is necessary to continue examination of the method. The current study utilized a small amount of data available from the literature. Future work will involve searching for larger available fracture toughness results necessary to conduct further evaluation of the J-A_2 method.

References

[1] ASTM, Standard E399-08, Linear-Elastic Plane-Strain Fracture Toughness K_{Ic} of Metallic Materials. *Annual Book of ASTM Standards,* ASTM International.
[2] ASTM, Standard E1921-11, Standard Test Method for Determination of Reference Temperature, To, for Ferritic Steels in the Transition Range. *Annual Book of ASTM Standards,* ASTM International.
[3] Hutchinson, J.W., 1968. Singular Behavior at the End of a Tensile Crack Tip in a Hardening Material. *J. Mech. Phys. Solids* 16 (1): 13-31.

[4] Rice, J.R., and Rosengren, G.F., 1968. Plane Strain Deformation Near a Crack Tip in a Power-Law Hardening Material. *J. Mech. Phys. Solids* 16 (1): 1-12.
[5] Ritchie, R.O., Knott, J.F., and Rice, J.R., 1973. On the Relationship Between Tensile Stress and Fracture Toughness in Mild Steel. *Journal of the Mechanics and Physics of Solids*, Vol. 21: 395-410.
[6] Yang, S., Chao, Y.J., and Sutton, M.A., 1993. Higher Order Asymptotic Crack Tip Fields in a Power-Law Hardening Material. *Engineering Fracture Mechanics* 45 (1): 1-20.
[7] Yang, S., Chao, Y.J., and Sutton, M.A., 1993. Complete Theoretical Analysis for Higher Order Asymptotic Terms and the HRR Zone at a Crack Tip for Mode I and Mode II Loading of a Hardening Material. *Acta Mechanica* 98 (1): 79-98.
[8] Chao, Y.J., Yang, S., and Sutton, M.A., 1994. On the Fracture of Solids Characterized by One or Two Parameters: Theory and Practice. *Journal of the Mechanics and Physics of Solids* 42 (1): 629-647.
[9] Chao, Y.J. and Ji, W., 1995. Cleavage Fracture Quantified by J and A2. *Constraint Effects in Fracture Theory and Applications: Second Volume.* ASTM STP 1244, Mark Kirk and Ad Bakker, Eds., American Society for Testing and Materials, Philadelphia, PA.
[10] Hohe, J., Hebel, J., Friedmann, V., and Siegele, D., 2007. Probabilistic failure assessment of ferritic steels using the master curve approach including constraint effects. *Engineering Fracture Mechanics* 74: 1274-1292.
[11] Hohe, J., Luckow, S., Hardenack, V., Sguaizer, Y., and Siegele, D., 2011. Enhanced fracture assessment under biaxial external loads using small scale cruciform bending specimens. *Engineering Fracture Mechanics* 78: 1876-1894.
[12] Scibetta, M., Schuurmans, J., and Lucon, E., 2008.Experimental Study of the Fracture Toughness Transferability to Pressurized Thermal Shock Representative Loading Conditions. *Journal of ASTM International* 5 (9): 1-14.
[13] Chao, Y.J. and Zhang, Li, 1997. *ME-Report 97-1: Tables of Plane Strain Crack Tip Fields: HRR and Higher Order Terms*. Department of Mechanical Engineering, University of South Carolina.
[14] Abaqus, 2010. *Abaqus/CAE User's* Manual. Version 6.10.
[15] Ritchie, R.O., Server, W.L., and Wullaert, R.A., 1979. Critical Fracture Stress and Fracture Strain Models for the Prediction of Lower and Upper Shelf Toughness in Nuclear Pressure Vessel Steels. *Metallurgical Transactions A* 10A: 1557-1570.
[16] Bates, R.C., 1987. Micromechanical Modeling for Prediction of Lower Shelf, Transition Region, and Upper Shelf Fracture Properties. *Fracture Mechanics: Microstructure and Micromechanisms (Papers presented at the 1987 ASM Material Science Seminar)* 1: 131-168.
[17] Wang, Z.X., Li, H.M., Chao, Y.J., and Lam, P.S., 2008. *Prediction of Characteristic Length and Fracture Toughness in Ductile-Brittle Transition (PVP2008-61608).* 2008 ASME Pressure Vessels and Piping Division Conference, Chicago, Illinois.
[18] Hohe, J., Hebel, J., Friedmann, V., and, Siegele, D., 2007. Probabilistic failure assessment of ferritic steels using the master curve approach including constraint effects. *Engineering Fracture Mechanics* 74 (1): 1274-1292.
[19] Lidbury, D. P. G., Sherry, A. H., Bass, B. R., Gilles, P., Connors, D., Eisele, U., Keim, E., Keinanen, H., Wallin, K., Lauerova, D., Marie, S., Nagel, G., Nilsson, K., Siegle, D., Wadier, Y., 2006. Validation of constraint-based methodology in structural integrity of ferritic steels for nuclear reactor pressure vessels. *Fatigue and Fracture of Engineering Materials & Structures* 29: 829-849.
[20] Keim, E., RPV integrity assessment using advanced fracture mechanics tools and multi scale modeling. *Regional workshop on Structural Integrity on LWR, Belo Horizonte, Brazil, 23-26 June 2009.*